Geophys. J. Int. (2004) **158,** 864–873 doi: 10.1111/j.1365-246X.2004.02343.x

The poloidal geomagnetic field in a differentially rotating upper core layer

H. Greiner-Mai,[1] L. Ballani[1] and D. Stromeyer[2]

[1]*Department Geodesy & Remote Sensing, GeoForschungsZentrum Potsdam (GFZ), Telegrafenberg,* D-14473 *Potsdam, Germany. E-mail: grm@gfz-potsdam.de*

[2]*Department Geomechanics & Geotechnology, GeoForschungsZentrum Potsdam (GFZ), Telegrafenberg,* D-14473 *Potsdam, Germany*

Accepted 2004 March 18. Received 2004 February 19; in original form 2003 July 10

SUMMARY

This paper deals with the inverse solution of the induction equation accounting for *moving* core material. In a layer of the fluid outer core we prescribe the associated velocity field by a differential rotation. The angular velocity near the core–mantle boundary (CMB) corresponds to the mean westward drift of the geomagnetic field. We solve the induction equation for the poloidal magnetic field in both the mantle and the fluid outer-core layer using the magnetic field as the boundary value at the Earth's surface and the assumed velocity field as the prescribed model parameter. The numerical solution of the induction equation is based on a modified Tikhonov regularization of an integral equation approach described in a previous paper by Ballani *et al.*.

This numerical experiment shows both the scope of our method with respect to highly conducting material and the effect of the motion of the conducting material on the penetration behaviour of field variations.

The results indicate that the downward continuation of the field by our method is possible to about 100 km below the CMB in the decadal time scale. The penetration depth mainly depends on the high conductivity, while the effect of the relative rotation is marginal in the uppermost 25 km and becomes more significant in deeper parts. Solutions become more unstable for depths of the outer core below 100 km, and no relevant solution fitting the data within 10 per cent can be reached, i.e. decadal field variations at these depths cannot be fully causally related to those observed at the Earth's surface.

Key words: core–mantle boundary, downward continuation, fluid outer core, induction equation, internal magnetic field, inverse problem.

1 INTRODUCTION

The determination of physical quantities near the core–mantle boundary (CMB) and the solution of some problems of core dynamics require the geomagnetic field in the CMB region to be inferred from its representations at the Earth's surface by inverse solutions of the induction equation. The electromagnetic (EM) core–mantle coupling torques and the velocity field of the core fluid are such quantities. The magnetic field in the CMB region must also be known as the boundary value of the dynamo problem and for studying filter properties of the CMB region on different timescales.

The electrical conductivity, σ, of this region must be known for the non-harmonic downward continuation by inverse solution. A constant value of the order of 10^5 S m^{-1} is widely accepted for the core part of this region. The situation is more complicated for the lower mantle, and the genesis of a lower-mantle conductivity of significant magnitude has not previously been adequately explained. The results of recent laboratory investigations go from low (Shankland *et al.* 1993) to high (Dubrovinsky *et al.* 2003) values. Laboratory experiments, however, cannot say anything about the spatial distribution of the conducting material, etc. The problems involved in condensing such information into a conductivity model practically applicable in a mathematical algorithm are discussed in greater detail in Section 4.

A perturbation method (e.g. Benton & Whaler 1983) has been developed previously by which the geomagnetic field can be continued downwards non-harmonically through weakly conducting regions of the mantle. The associated series solution of the induction equation requires the time derivatives of the Gauss coefficients of the geomagnetic field as input parameters. These coefficients are inferred as 'model data' from geomagnetic measurements. Consequently, the convergence of the solution can never be proved theoretically and depends on both the spatial and temporal scales of the available representation of the observed field and the assumed value of mantle conductivity. Within this framework, the non-harmonically downward-continued field is necessary to compute EM torques. The

harmonically continued components of the geomagnetic and the secular variation (sv) field, B_r^0 and $\dot{B}_r^0$, have been used up to now to determine the velocity field at the top of the core by inversion of the frozen-flux equation.

Exploring the scope of these approximations for parts of the CMB region with higher conductivity and defining the corresponding parameter ranges is, however, not the purpose of this paper. This has been done recently by Ballani *et al.* (2002). In this paper, we will present and use an algorithm for the full numerical solution of the total induction equation to infer the poloidal geomagnetic field in the CMB region. This method works without assumptions about the magnitude of σ and the space–time scale of the observed field: the method is based on the inversion technique applied to one-sided initial boundary value problems (e.g. Eldén 1995), leading to a comprehensive spatiotemporal solution. The solution no longer requires 'data' about the secular variation field or higher-time derivatives of **B**, which contain no additional and/or independent information about the geomagnetic field anyway.

Ballani *et al.* (1995, 2002) have recently developed such a method for the non-harmonic downward continuation of the geomagnetic field to the CMB ($r = R_c$). Its theoretical framework is based on the following findings. For the mantle, the induction equation for the poloidal geomagnetic field $\mathbf{B}_p$ can be decomposed into decoupled differential equations of second order for the spherical harmonic modes, S_{nm}, of the poloidal field scalar, S, defining the poloidal magnetic field by

$$\mathbf{B}_p = \text{curl curl } (\mathbf{r}S), \tag{1}$$

where **r** is the position vector. The associated initial boundary value problem is related to the model geometry shown in Fig. 1. The two boundary conditions ('model data') are given by the Gauss coefficients of the geomagnetic potential field, g_{nm} and h_{nm}, at the Earth's surface, $r = R_E$. The mantle is approximated by an outer insulating shell of radius R_σ and an inner electrically conducting shell beginning below R_σ. Within the insulating shell, the magnetic field behaves like a potential field and can be harmonically continued downwards to $r = R_\sigma$. Therefore, the sphere $r = R_\sigma$ appears as the actual boundary for the governing differential equation for $\sigma \neq 0$.

The mathematical problem of solving the induction equation for $r \in [R_c, R_\sigma]$ with data given only at one side is then an inverse problem which is severely ill-posed. To obtain an optimal solution, Ballani *et al.* (2002) have transformed the induction equation into a Volterra equation of the first kind (Eldén 1995) and solved a regularizing optimal control problem for the unknown boundary function $S_{nm}(R_c, t)$ (Section 3). The solution procedure is based on the related, well-developed, inverse heat conduction theory (Dinh Nho Hào & Gorenflo 1991; Reinhardt & Seiffarth 1993). To overcome the difficulties with a space-variable coefficient function in the differential equation, the solution algorithm uses an idea developed for geothermal inversion (Stromeyer 1983, 1984).

Apart from the computation of the field at the CMB, Ballani *et al.* (2002) have tested their algorithm for highly conducting layers by calculating S_{nm} in a thin non-moving (passive) upper core layer, $r \in [R_c, R_{oc}]$. This is motivated by hypotheses about sedimentation of light elements in the core producing a shell of highly conducting material covering the CMB at the core side (e.g. Buffett *et al.* 2000). The motion with the velocity field, **v**, responsible for the geomagnetic sv then starts below such layers at $R_{oc} < R_c$, i.e. the component B_r necessary for the frozen-flux estimate of **v** must be continued through this layer. A comprehensive method to estimate B_r at R_{oc} is most important, in particular, for modelling events with mixed timescales (high and low frequencies) like the geomagnetic jerk (Ballani *et al.* 2004).

In this paper we will extend this method to calculations of S_{nm} in a core shell in which the electrically conducting liquid rotates differentially with the angular velocity $\omega(r)$. This assumption is motivated by an objective which can only be reached in the future: a joint inversion of the core induction equation in deeper core parts with respect to $\mathbf{B}_p$ *and* **v**. This is still out of our reach at the moment as it will require an additional dynamic concept constraining **v** physically, e.g. at $r = R_{oc}$. First investigations in this direction are the trials to invert the dynamo equations (Stefani & Gerbeth 2000a,b).

To assume a differential rotation should be understood as a first step by which (1) a numerical algorithm of the inverse solution of the induction equation for this moving core fluid with its prescribed velocity field is found and tested and (2) the effect of the motion on the diffusion of magnetic field variations through the outermost parts of the core will be studied. The latter might also be valuable to evaluate the maximum depth of the processes causing the observed decadal variations of the geomagnetic field (defined by their electromagnetic penetration power). Some additional physical reasoning for assuming a differential rotation is given in Section 4.

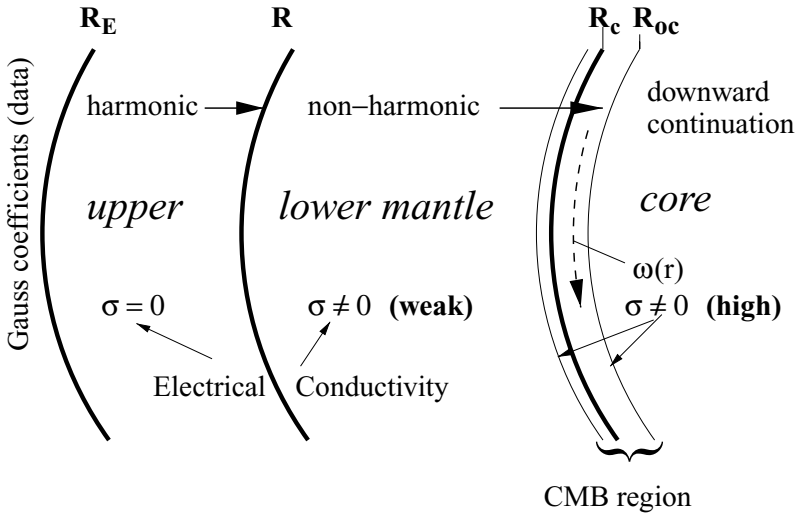

Figure 1. The boundary data and model geometry: radii used $R_\sigma = 5480$ km, $R_c = 3485$ km, $R_{oc} = R_c - 25$, -50 and -100 km; see Section 4 for σ and ω values.

From a mathematical point of view, the choice of a differential rotation is somewhat pragmatic: for the associated velocity field, $\mathbf{v} = \boldsymbol{\omega} \times \mathbf{r}$, $\boldsymbol{\omega} = (0, 0, \omega)$, the induction equation can be decomposed into two independent systems of differential equations for the poloidal and the toroidal magnetic field, respectively. This ensures that the poloidal magnetic field can be calculated without information about the toroidal field $\mathbf{B}_t$. It is not considered here because further modelling and additional assumptions are necessary to *calculate* its boundary values at $r = R_c$, R_{oc}. Inference from surface data is impossible, because $\mathbf{B}_t$ is zero if σ is zero.

Although the conductivity of the core is assumed to be constant, the velocity parameter $\omega(r)$ reintroduces an additional r-dependent coefficient into the differential equations of the core, and couples the sine and cosine modes appearing here as imaginary and real parts, respectively, of a complex spherical harmonic mode. The algorithm applied by Ballani *et al.* (2002) to non-rotating shells must therefore be modified. The terminology 'inverse' is used here with respect to the determination of $\mathbf{B}_p$ and not of $\mathbf{v}$. For the inversion of the core induction equation with respect to $\mathbf{v}$ (but not $\mathbf{B}$) with the diffusion term considered, we refer to an approximation given by Gubbins (1996).

2 INDUCTION EQUATION OF AN AXIALLY ROTATING FLUID

In the following, we outline the derivation of the scalar induction equation given in textbooks, e.g. Krause & Rädler (1980). The vectorial induction equation for a moving fluid is given by

$$-\text{curl}\left(\frac{1}{\mu_0\sigma}\text{curl}\,\mathbf{B}\right) + \text{curl}\,(\mathbf{v}\times\mathbf{B}) = \dot{\mathbf{B}}$$
$$\text{div}\,\mathbf{B} = 0 \tag{2}$$

where μ_0 is the permeability of vacuum, σ is the electrical conductivity (constant in the core), $\mathbf{B}$ is the magnetic flux density and $\mathbf{v}$ is the velocity field of moving material. $\mathbf{B}$ can be decomposed into its poloidal and toroidal part, $\mathbf{B}_p$ and $\mathbf{B}_t$

$$\mathbf{B} = \mathbf{B}_p + \mathbf{B}_t = \text{curl curl}\,(\mathbf{r}S) + \text{curl}\,(\mathbf{r}T) \tag{3}$$

which are represented by scalar functions S and T, which average to zero on spheres for normalization. The term $\mathbf{v}\times\mathbf{B}$ can be written by the decomposition

$$\mathbf{v}\times\mathbf{B} = \text{curl}\,\mathbf{r}\,U + \mathbf{r}\,V + \text{grad}\,W. \tag{4}$$

It defines a representation of a vector field with non-vanishing divergence by three scalar functions, two of which (U, V) shall be normed by $\oint \ldots \sin\vartheta\, d\vartheta\, d\varphi = 0$, like S and T. We obtain from eq. (2) with eqs (3) and (4) the poloidal scalar induction equation at a preliminary stage:

$$\frac{1}{\mu_0\sigma}\Delta S + U = \dot{S}. \tag{5}$$

This connects the poloidal scalar S in eq. (3) with the scalar U of the toroidal part of $\mathbf{v}\times\mathbf{B}$ in eq. (4). To introduce $\mathbf{v}$ in a special form we take the radial component of curl($\mathbf{v}\times\mathbf{B}$), finding the equation

$$\mathcal{L}^2 U = -\mathbf{r}\,\text{curl}\,(\mathbf{v}\times\mathbf{B}), \tag{6}$$

where

$$\mathcal{L}^2 = \frac{1}{\sin\vartheta}\frac{\partial}{\partial\vartheta}\left(\sin\vartheta\frac{\partial}{\partial\vartheta}\right) + \frac{1}{\sin^2\vartheta}\frac{\partial^2}{\partial\varphi^2} \tag{7}$$

is the Laplacian at a sphere $r = \text{const}$. Using the poloidal part in eq. (3) there results for a rotating fluid with $\mathbf{v} = \boldsymbol{\omega}\times\mathbf{r}$, $\boldsymbol{\omega}$ the vector of the angular velocity, the relation

$$\mathcal{L}^2 U = -\boldsymbol{\omega}(r)(\mathbf{r}\times\text{grad}\,\mathcal{L}^2 S). \tag{8}$$

In the axisymmetric case $\boldsymbol{\omega} = (0, 0, \omega(r))$ to be applied here, it is simplified to

$$\mathcal{L}^2 U = -\left(\frac{\partial\mathcal{L}^2 S}{\partial\varphi}\right)\cdot\omega(r). \tag{9}$$

Due to the normalization conditions for U, S with eq. (9) the relation

$$U = -\left(\frac{\partial S}{\partial\varphi}\right)\cdot\omega(r) \tag{10}$$

holds. Therefore, the scalar induction equation (eq. 5) can be written in the final form

$$\frac{1}{\mu_0\sigma}\Delta S - \left(\frac{\partial S}{\partial\varphi}\right)\cdot\omega(r) = \dot{S}. \tag{11}$$

By spherical harmonic expansion of S we introduce the complex spherical harmonic modes S_{nm}

$$S(r,\vartheta,\varphi,t) = \sum_{n,m} S_{nm}(r,t)Y_{nm}(\vartheta,\varphi) \tag{12}$$

where the spherical surface harmonics Y_{nm} are given (e.g. Arfken 1966) by

$$Y_{nm}(\vartheta,\varphi) = P_{nm}(\cos\vartheta)e^{im\varphi}. \tag{13}$$

The P_{nm}, $n \geq m \geq 0$, are the associated Legendre functions defined by

$$P_{nm}(\mu) = \frac{(1-\mu^2)^{m/2}}{2^n n!}\frac{d^{n+m}}{d\mu^{n+m}}(\mu^2-1)^n \tag{14}$$

and extended for a negative second index $-m$ to

$$P_{n,-m}(\mu) = (-1)^m\frac{(n-m)!}{(n+m)!}P_{nm}(\mu). \tag{15}$$

As the poloidal scalar S in eq. (12) should be real, we have to require for the modes

$$S_{n,-m} = (-1)^m\frac{(n+m)!}{(n-m)!}S^*_{nm} \tag{16}$$

where the asterisk denotes complex conjugation. Y_{nm} are the eigenfunctions of $\mathcal{L}^2$ with the corresponding eigenvalues $-n(n+1)$. Thus the Y_{nm} can be used to decompose the scalar induction eq. (11) into a set of single, decoupled differential equations for the modes $S_{nm}(r,t)$

$$\frac{\partial^2 S_{nm}}{\partial r^2} + \frac{2}{r}\frac{\partial S_{nm}}{\partial r} - \left(\frac{n(n+1)}{r^2} + im\mu_0\sigma(r)\omega(r)\right)S_{nm}$$
$$= \mu_0\sigma(r)\frac{\partial S_{nm}}{\partial t} \tag{17}$$

For each n, m this equation now represents a special portion of the mantle–core induction equation to be applied in the following.

3 THE ALGORITHM FOR SOLVING THE MANTLE–CORE INDUCTION EQUATIONS

We consider the problem of downward continuation of the geomagnetic field measured at the Earth's surface down to a level R_{oc} beneath the CMB in the fluid outer core. Boundary values, here applied in the form of Gauss coefficients $g_{nm}(t)$, $h_{nm}(t)$, only exist as outer boundary values on the Earth's surface R_E, or by conventional

analytic (harmonic) downward continuation for a deeper radius, R_σ. Therefore, this problem can be characterized as an inverse boundary value problem to determine the time function $S_{nm}(R_{oc}, t)$ at the boundary R_{oc} from

$$\frac{\partial^2 S_{nm}}{\partial r^2} + \frac{2}{r}\frac{\partial S_{nm}}{\partial r} - \left(\frac{n(n+1)}{r^2} + im\mu_0\sigma(r)\omega(r)\right) S_{nm} = \mu_0\sigma(r)\frac{\partial S_{nm}}{\partial t} \tag{18}$$

$$S_{nm}(R_\sigma, t) = \phi(t), \quad \frac{\partial S_{nm}(R_\sigma, t)}{\partial r} + \frac{n+1}{R_\sigma} S_{nm}(R_\sigma, t) = 0, \quad 0 \le t \le T \tag{19}$$

$$S_{nm}(r, 0) = \psi(r), \qquad R_{oc} \le r \le R_\sigma. \tag{20}$$

The relations (19) formulate the *two outer boundary conditions*. The second one is derived from the continuity of $\partial/\partial r(rS_{nm})$ at the transition R_σ between non-conducting and conducting mantle shell. The first boundary condition is given in detail by

$$\phi(t) = \frac{\lambda_{nm}}{2-\delta_{0m}} \frac{R_E^{n+2} R_\sigma^{-n-1}}{n} (g_{nm}(t) - \mathrm{i}h_{nm}(t)), \quad n \ge 1, n \ge m \ge 0 \tag{21}$$

(with δ_{nm} the Kronecker delta and $h_{n0}(t) \equiv 0$) where λ_{nm} are the Schmidt's normalization coefficients

$$\lambda_{nm} = \left((2-\delta_{0m})\frac{(n-m)!}{(n+m)!}\right)^{1/2}. \tag{22}$$

Eq. (20) is the *initial condition*. It can be arbitrarily chosen, e.g. as solution $\psi(r)$, $R_{oc} \le r \le R_\sigma$, of the equation

$$\frac{\partial^2 \psi}{\partial r^2} + \frac{2}{r}\frac{\partial \psi}{\partial r} - \left(\frac{n(n+1)}{r^2} + im\mu_0\sigma(r)\omega(r)\right)\psi = 0 \tag{23}$$

which gives the known harmonic (analytic) potential solution valid for an insulator $\psi(r) \propto r^{-n-1}$ for the partial mantle interval $R_c \le r \le R_\sigma$ ($\omega(r) \equiv 0$ or $\sigma \equiv 0$). However, for the whole r interval, $R_{oc} \le r \le R_\sigma$, $\psi(r)$ has to be determined by numerical integration of these ordinary differential equations.

The following *special cases of downward field continuation* can help to elucidate and to understand the comparative results given below as well as to classify earlier work (Ballani *et al.* 2002):

(1) The simplest and most commonly used downward field continuation is the harmonic one using

$$\sigma(r) \equiv 0 \text{ in eq. (18)} \left(\text{followed by } \omega(r) \equiv 0, \frac{\partial}{\partial t} = 0\right). \tag{24}$$

It is described by the separation solution $G_{nm}(t) \cdot F_n^{\mathrm{harm}}(r)$ of eq. (18) where the harmonic function $F_n^{\mathrm{harm}}(r)$ is a solution of the ordinary differential equation (eq. 23) for $\sigma \equiv 0$. $G_{nm}(t)$ contains the upper boundary time structure; here, for example, that of Gauss coefficients.

(2) Determining the poloidal field at and beneath the CMB, $R_{oc} \le R_c$, assuming in eq. (18)

$$\sigma(r) \ne 0, \qquad \omega(r) \equiv 0, \qquad \frac{\partial}{\partial t} \ne 0, \tag{25}$$

provides decoupled equations for the real and imaginary part of S_{nm} to be continued downwards through the Earth's mantle and deeper to a passive (non-moving) layer on top of the fluid outer core (Ballani *et al.* 2002).

(3) The special case of harmonic downward continuation (eq. 1) belongs to the more general class of the 'steady-state field downward continuation' which works under the assumption that the diffusion term in the right-hand side of eq. (18) is omitted

$$\sigma(r) \ne 0, \qquad \omega(r) \ne 0, \qquad \frac{\partial}{\partial t} = 0 \tag{26}$$

As for eq. (24) $G_{nm}(t) \cdot F_{nm}^{\mathrm{steady}}(r)$ is obtained as the separation solution of eq. (18) where $F_{nm}^{\mathrm{steady}}(r)$ is a solution of the ordinary differential eq. (23). $G_{nm}(t)$ is preserving the time structure of the upper boundary, which is the main characteristic of the steady-state downward continuation.

(4) Preserving the time structure is no longer true in the more general boundary value problem, eqs (18), (19), (20), with

$$\sigma(r) \ne 0, \qquad \omega(r) \ne 0, \qquad \frac{\partial}{\partial t} \ne 0 \tag{27}$$

whose solution in the following will be called 'diffusive downward continuation' (up to now the term 'non-harmonic downward continuation' has been used simply for distinction).

The *basic properties* of the general diffusive downward continuation problem, eqs (18), (19), (20), which is equipped with parameter functions, the conductivity $\sigma(r)$ and the fluid velocity $\omega(r)$, are its uniqueness and its instability concerning the higher-frequency part of the temporal spectrum. Both properties are important for constructing a solution algorithm which needs a regularizing procedure.

The *algorithm* for the solution of eqs (18), (19), (20) is based on the equivalent form of an integral equation of the first kind. It describes the linear relation between pure time functions in $0 \le t \le T$ for the two different r levels: the known function (data) at R_σ,

$$\phi(t) = S_{nm}(R_\sigma, t), \tag{28}$$

and the unknown function (solution) at R_{oc},

$$f(t) = S_{nm}(R_{oc}, t). \tag{29}$$

The solution function is expanded by a finite set of linearly independent functions (basis) and is searched for as a minimum norm solution with a special regularization variant.

The three *solution steps* in detail are the following:

Step (i): The problem of eqs (18), (19), (20) is transformed so that the resulting problem has the zero initial condition. For that, we solve the following stable two-sided boundary value problem:

$$\frac{\partial^2 V}{\partial r^2} + \frac{2}{r}\frac{\partial V}{\partial r} - \left(\frac{n(n+1)}{r^2} + im\mu_0\sigma(r)\omega(r)\right) V = \mu_0\sigma(r)\frac{\partial V}{\partial t} \tag{30}$$

$$V(R_{oc}, t) = 0, \quad \frac{\partial V}{\partial r}(R_\sigma, t) + \frac{n+1}{R_\sigma} V(R_\sigma, t) = 0, \quad 0 \le t \le T \tag{31}$$

$$V(r, 0) = \psi(r), \qquad R_{oc} \le r \le R_\sigma \tag{32}$$

with the same initial condition eq. (32) as the original problem eq. (20) and homogeneous boundary conditions at the lower side R_{oc} (first part of eq. 31) and the same as the second one in eq. (19) at R_σ. Now, for the difference function

$$S_{nm}^V = S_{nm} - V \tag{33}$$

an inverse boundary value problem in full analogy to eqs (18), (19), (20) can be considered. S_{nm}^V again fulfils the original

differential eq. (18), the second boundary condition of eq. (19) and—as intended—the zero initial condition

$$S^V_{nm}(r,0) = 0, \qquad R_{\rm oc} \le r \le R_\sigma. \tag{34}$$

The first boundary condition of eq. (19), as the data input, is now changed to

$$S^V_{nm}(R_\sigma, t) = \phi(t) - V(R_\sigma, t), \qquad 0 \le t \le T \tag{35}$$

where $V(R_\sigma, t)$ is the solution of eqs (30), (31), (32) to be determined. The first condition in eq. (31) means that this transformation does not change the unknown function

$$S_{nm}(R_{\rm oc}, t) = S^V_{nm}(R_{\rm oc}, t). \tag{36}$$

In the following, considering the transformed inverse boundary value problem for $S^V_{nm}(R_{\rm oc}, t)$, we will return to the original notation: omitting the superscript V and denoting the changed boundary condition eq. (35) simply by $\phi(t)$ again. By the zero initial condition the equivalent integral equation for our problem, eqs (18), (19), (20), is now a convolution type Volterra equation of the first kind

$$\phi(t) = A(f(t)) = \int_0^t k(t-\tau) f(\tau)\, d\tau,$$
$$\phi(t) = S_{nm}(R_\sigma, t), \quad f(t) = S_{nm}(R_{\rm oc}, t). \tag{37}$$

Obviously, the kernel $k(t)$ contains all the dependences on r, R_σ, $R_{\rm oc}$, n, m, $\sigma(r)$ and $\omega(r)$. However, for $\sigma(r)$, $\omega(r) \neq$ const, the kernel can no longer be specified analytically. Therefore, the upward continuation operator A cannot really be calculated in this way, but shall be tackled in combination with function bases.

Step (ii): The time function $f(t) = S_{nm}(R_{\rm oc}, t)$ is expanded by basis functions $\{e_k(t)\}$

$$f(t) = \sum_k f_k e_k(t) \tag{38}$$

Its upward continuation

$$A(f(t)) = \sum_k f_k A(e_k(t)) \tag{39}$$

can then be described as a linear combination of upward-continued individual basis functions

$$e^\sigma_k(t) = A(e_k(t)). \tag{40}$$

For their determination we solve the following (stable) boundary value problems for the induction equation which is the inversion of the downward continuation problem of the type in eqs (18), (19), (20) due to uniqueness:

$$\frac{\partial^2 U_k}{\partial r^2} + \frac{2}{r}\frac{\partial U_k}{\partial r} - \left(\frac{n(n+1)}{r^2} + im\mu_0\sigma(r)\omega(r)\right) U_k = \mu_0\sigma(r)\frac{\partial U_k}{\partial t}$$

$$U_k(R_{\rm oc}, t) = e_k(t) \tag{41}$$

$$\frac{\partial U_k}{\partial r}(R_\sigma, t) + \frac{n+1}{R_\sigma} U_k(R_\sigma, t) = 0, \qquad 0 \le t \le T$$

$$U_k(r, 0) = 0, \qquad R_{\rm oc} \le r \le R_\sigma.$$

The time function

$$e^\sigma_k(t) = U_k(R_\sigma, t) \tag{42}$$

is obtained as the solution. With another basis of time functions $\{\chi_i(t)\}$, it can be expanded as:

$$e^\sigma_k(t) = \sum_i a_{ik}\chi_i(t) = A(e_k(t)). \tag{43}$$

Obviously, the coefficients a_{ik} form the matrix which describes the operator A with respect to the bases $\{e_k(t)\}$ and $\{\chi_i(t)\}$. If we introduce $\{\phi_i\}$ as the expansion coefficients of the data function $S_{nm}(R_\sigma, t)$ by

$$S_{nm}(R_\sigma, t) = \phi(t) = \sum_i \phi_i \chi_i(t) \tag{44}$$

we find the corresponding matrix–vector relation for the coefficients (vectors) of known and unknown function

$$(\phi_i) = \sum_k a_{ik} f_k = (a_{ik})(f_k). \tag{45}$$

Step (iii): After the numerical determination of the matrix elements a_{ik} by eqs (41), (43) and of the data expansion coefficients (ϕ_i) from eq. (44), the expansion coefficients (f_k) of the time function $S_{nm}(R_{\rm oc}, t)$ (eq. 38) remain as the proper unknowns of the downward continuation problem. They are determined by a Tikhonov regularization of the type

$$\min \|(f_k)\|_\beta \quad \text{subject to} \quad \|(a_{ik})(f_k) - (\phi_i)\|_\alpha \le \epsilon \tag{46}$$

which accounts especially for the error ϵ of the data at R_σ (second term) while the first term searches for optimal temporal smoothness of the solution at the fixed r level, $R_{\rm oc}$, according to the applied norm $\|\cdot\|_\beta$. It means that this method does not regularize for smoothness in the space variable. The regularization procedure is implemented with the help of a quadratic programming tool of Hansen (1994) contained in the regularization toolbox. We select the norms $\|\cdot\|_\alpha$, $\|\cdot\|_\beta$ as L_2 and W^1_2 norms, respectively, referring only to the pure time function while r is a fixed parameter:

$$\|u(r,.)\|_2 = \left(\int_0^T |u(r,t)|^2\, dt\right)^{1/2} \qquad (L_2 \text{ norm}) \tag{47}$$

and

$$\|u(r,.)\|_{W^1_2} = \|u(r,.)\|_2 + \left\|\frac{\partial u}{\partial t}(r,.)\right\|_2 \qquad \left(W^1_2 \text{ norm}\right). \tag{48}$$

As the initial transform (i) with eq. (31) does not change the lower boundary value at $R_{\rm oc}$, the unknown function (eq. 36), the result of Step (iii), is already identical with the final solution.

In addition to this basic course (Steps (i), (ii) and (iii)), the algorithm can still be simplified considerably if some specializations are made in Step (ii). They can be introduced and treated by substitutions in the equation of the Volterra operator (eq. 37). Considering the interval $[0, T]$ we assume N as the number of basis functions $e_k(t)$ (see eq. 38) and abbreviate the length of a partial interval by $h = T/N$. We choose a 'first function' $e_1(t)$ which shall be a quadratically integrable function on $[0, T]$ with

$$e_1(t) = \begin{cases} \not\equiv 0 & \text{for} \quad 0 < t \le h \\ 0 & \text{for} \quad h < t \le T. \end{cases} \tag{49}$$

Then by successive shifting of $e_1(t)$

$$e_k(t) = \begin{cases} e_1(t-(k-1)h) & \text{for} \quad (k-1)h < t \le kh \\ 0 & \text{otherwise} \end{cases} \qquad k = 2, \ldots, N \tag{50}$$

an orthogonal function set $e_k(t)$, $k = 1, \ldots, N$ is generated. The associated upward-continued basis functions $e_k^\sigma = A(e_k)$, $k = 2, \ldots, N$, solutions of eq. (41), show a similar shift property, so that they all can be obtained by shifting of e_1^σ

$$e_k^\sigma(t) = \begin{cases} 0 & \text{for} \quad 0 < t \le (k-1)h \\ e_1^\sigma(t-(k-1)h) & \text{for} \quad (k-1)h < t \le T \end{cases} \qquad k = 2, \ldots, N. \tag{51}$$

This means that only $e_1^\sigma(t)$, the upward-continued first basis function $e_1(t)$, really has to be calculated.

If, in addition, the basis $\{\chi_i(t)\}$ (eq. 43) has the shift property of eq. (50), then both sets $\{e_k\}$, $\{\chi_i\}$ are orthogonal systems. The related matrix can be represented by

$$(a_{ik}) = (Ae_k, \chi_i) \tag{52}$$

where $(\cdot, \cdot)$ means the scalar product on $[0, T]$. From these properties it follows that (a_{ik}) is a Toeplitz matrix, i.e. for each i and k, $1 \le i$, $k \le N$ and any integer l, with $1 \le i + l \le N$ and $1 \le k + l \le N$, the typical Toeplitz diagonal property

$$a_{i+l,k+l} = a_{ik} \tag{53}$$

can be derived. Moreover, (a_{ik}) is also a lower triangular matrix, because

$$a_{ik} = 0 \quad \text{for} \quad k > i \tag{54}$$

holds, reflecting temporal causality. The main consequence of these assumptions is that it is sufficient to determine the first column (a_{i1}) of (a_{ik}), i.e. only one stable problem (eq. 41) ($k = 1$) really has to be solved.

Both bases $\{e_k(t)\}$, $\{\chi_i(t)\}$, which we will use in the following, have been selected to be identical and consisting of 'triangle functions'. They are generated by a first basis function $e_1(t)$

$$e_1(t) = \begin{cases} 2t/h & \text{for} \quad 0 \le t \le h/2 \\ 2 - 2t/h & \text{for} \quad h/2 < t \le h \\ 0 & \text{for} \quad h < t \le T \end{cases} \tag{55}$$

and then shifted by eq. (50) (the same for $\{\chi_i\}$). Such a basis has the advantage that it corresponds directly to an equidistant time discretization: the ith partial interval $[(i-1)h, ih]$ with length h is assigned to the time point t_i by $t_i = h(i - 1/2)$ so that this time point coincides with the maximum value ($= 1$) of the ith triangle function.

4 MODEL ASSUMPTIONS: DATA, CONDUCTIVITY AND VELOCITY MODELS

The data used are the Gauss coefficients given by Bloxham & Jackson (1992). On the basis of a spline interpolation, the coefficients are taken as equally spaced ($\Delta t = 2$ yr) covering the time interval 1690–1990. As an example, we demonstrate the downward continuation for the Gauss coefficient g_{11}. To present our downward continuation result, we define the time functions g_{nm}^{oc} as

$$g_{nm}^{\mathrm{oc}}(t) = \frac{n}{\lambda_{nm}} \frac{2 - \delta_{0m}}{R_{\mathrm{E}}} \mathrm{Re}\{S_{nm}(R_{\mathrm{oc}}, t)\} \tag{56}$$

which depend on one of the three different angular velocity models $\omega(r)$ respectively (see Fig. 2).

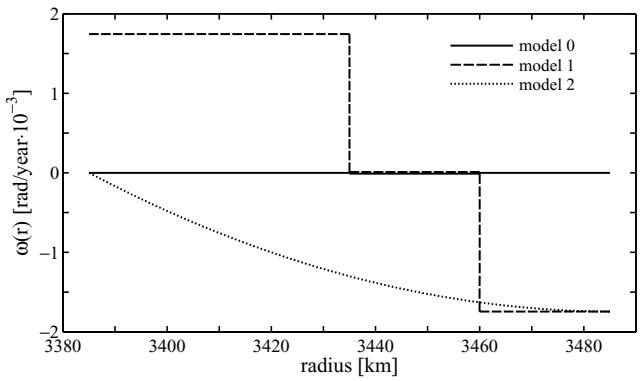

Figure 2. Velocity models: prescribed dependence of the angular velocity, ω, on radius r.

For the steady-state downward continuation (see eq. 26) we have

$$g_{nm}^{\mathrm{oc}}(t) = F_{nm}^{\mathrm{steady}}(R_{\mathrm{oc}}) \cdot g_{nm}(t) \tag{57}$$

where $F_{nm}^{\mathrm{steady}}(r)$ is the solution of eq. (23) for given n, m and depends on the ω model. If $\omega \equiv 0$ (model 0) is selected, which is the harmonic case (see eq. 24), the relation

$$F_{nm}^{\mathrm{steady}}(R_{\mathrm{oc}}) = \left(\frac{R_{\mathrm{E}}}{R_{\mathrm{oc}}}\right)^{n+1} \tag{58}$$

is valid.

In addition, we calculate the radial field component, B_{r}, up to degree 8

$$B_{\mathrm{r}}(r, \vartheta, \varphi, t) = \frac{1}{r} \sum_{n=1}^{8} n(n+1) \sum_{m=0}^{n} (2 - \delta_{0m}) \mathrm{Re}\{S_{nm}(r, t) Y_{nm}(\vartheta, \varphi)\} \tag{59}$$

at different core depths, which is completely determined by the poloidal part of **B**.

For the numerical method used, it is necessary that the model of the electrical conductivity of the core–mantle region approximates some findings about this region by spherical shells, in which σ is constant or dependent on r. Recent investigations of this region suggest that it is a complex transition zone including several kilometres of the upper core (e.g. Buffett *et al.* 2000) and a few hundred kilometres of the lower-most mantle (e.g. Lay *et al.* 1998), the so-called D″ layer, which can be the result of, for example, compositional variation, partial melting or infiltration of core material producing a laterally heterogeneous high-conductivity layer in the lower mantle.

Although a comprehensive model of this layer and its electrical conductivity has not yet been developed, a layer with a high conductance is suggested by the phase behaviour of the Earth's nutation (Buffett 1992) and EM core–mantle coupling on decadal time scales (e.g. Holme 1998). The necessary conductance can be reached by either a thin shell with mantle conductivity, σ_{M}, of the order of the core conductivity or a thicker shell with lower conductivity (maximum thickness like D″). A conductivity value of the order of magnitude of that of the core was recently determined by laboratory experiments (Dubrovinsky *et al.* 2003) as a realistic assumption.

Therefore, in the model below we assume a thin layer of 2 km at the bottom of the mantle having a conductance of 2×10^8 S, which is of the order of that necessary for EM core–mantle coupling. In the end, this and a possible lateral structure has no significant effect on our investigation because the major effect is that of core conductivity—the thin layer and the overlying layer with $\sigma_{\mathrm{M}} \propto (R_{\mathrm{c}}/r)^5$ are added

for consistency with core–mantle coupling, not considered here, and completeness.

In this paper, the conductivity model is prescribed by

$$\sigma(r) = \begin{cases} 0 & R_\sigma < r \\ 10 \times (R_c/r)^5 & R_c + 2\ \text{km} < r \le R_\sigma \\ 1 \times 10^5 & R_c \le r \le R_c + 2\ \text{km} \\ 2 \times 10^5 & R_c > r, \end{cases} \tag{60}$$

where the unit of $\sigma(r)$ is S m^{-1} and the basic radii are taken as $R_\sigma =$ 5480 km and $R_c = 3485$ km. The first three shells give the conductivity of the mantle, σ_M, the last that of the core. For the region in the interval $R_c + 2\ \text{km} < r \le R_\sigma$, σ_M is chosen according to the results from laboratory experiments (e.g. Shankland *et al.* 1993). The effect of this shell on the inverse solution is marginal on the decadal timescale because its conductance is about two orders lower than that of the thin shell at the bottom of the mantle. This lower-most shell of the mantle in eq. (60) ensures the conductance necessary for the EM core–mantle coupling and decadal length-of-day variations. Its value can also be reached by other combinations of the thickness of the shell and the value of σ_M. Apart from this, the assumed model (eq. 60) should be considered primarily as an example for which the numerical algorithm will be demonstrated. Nevertheless, the model of mantle conductivity (homogeneity and thickness of the shell) must be constructed more carefully, if short-period phenomena are to be described, like nearly diurnal oscillations in the core rotation (e.g. Buffett *et al.* 2002) or jerks (Backus 1983). The problem becomes seriously difficult for significantly heterogeneous conductivity distributions because then the differential equations for the poloidal and toroidal field are coupled, and the toroidal field is zero at the interface between a conductor and insulator.

The main objective of this paper is to test the new algorithm of field continuation into the core for moving core material and to choose as a first approach a rigid r-dependent rotation. It is not our intention to give the physical reasoning for such an assumption which is completely consistent with core dynamics. Indications of the assumption of a passive or relatively rotating upper-core layer are given by the sedimentation hypothesis of Buffett *et al.* (2000), the H-layer of Braginsky (1993) and other hypotheses of stably stratified states of the upper core, which can break down from time to time (Bellanger *et al.* 2001), to give an explanation of the origin of geomagnetic jerks.

Further physical motivations behind the choice of a rotational state are given by hypotheses about (1) stable stratification and torsional oscillation of such a shell (e.g. Braginsky 1993; Tanaka & Hamaguchi 1993) and (2) the need of an outer-core shell (thickness d) to balance the axial component of the angular momentum derived from variations of the length of day (e.g. Greiner-Mai 1995).

What in fact can be inferred from observations is the angular velocity, ω, at or near the top of the core by frozen-flux inversion. To determine ω in deeper parts is a matter of core dynamics and is not considered here. Therefore, we can adopt the core-surface value of ω in accordance with frozen-flux theory, but must prescribe $\omega(r)$ in deeper parts at this stage of investigation.

For the value of the velocity function $\omega(r)$ at the CMB, we choose the mean westward drift of the outer core, $\omega = -0.1^\circ$ yr^{-1} (e.g. Greiner-Mai 1986). Further, we prescribe the radial dependence of ω for $r \in (R_c - 100\ \text{km}, R_c)$ by the alternative possibilities of (1) a step function and (2) a continuous increase to zero, both shown in Fig. 2. The step function includes a partial eastward drift in deeper parts and the results will show the effect of this change of the sign of ω. The model assumptions about $\omega(r)$ imply that the observed variations (except for a global drift) are caused by processes (sources of the secular variation) in core parts lying deeper than the respective R_{oc} value.

We choose a maximum depth of 100 km, because the skin depth is about 20 to 60 km for periods of 20 to 100 yr and we expect that the solution becomes unstable for $r < R_c - 100$ km. The results for three velocity models (see eqs 27, 25) are then compared with the inverse solutions for their steady-state counterparts (see eqs 26, 24). The last case (eq. 24) corresponds to the potential solution.

5 RESULTS

Fig. 3 shows the resulting variations of the poloidal g_{11} modes at several radii, $R_{oc} \le R_c$, and for the different ω as an example. In addition, Figs 4 and 5 show the influence of the relative rotation on the continued field, demonstrated by the difference of the radial component, B_r, of **B** between the ω models 1, 2 and the ω model 0, i.e. between the rotating and non-rotating state.

Following Fig. 2, the ω models 0, 1, 2 will in the following be denoted as model 0, 1, 2. In this section, we will discuss the

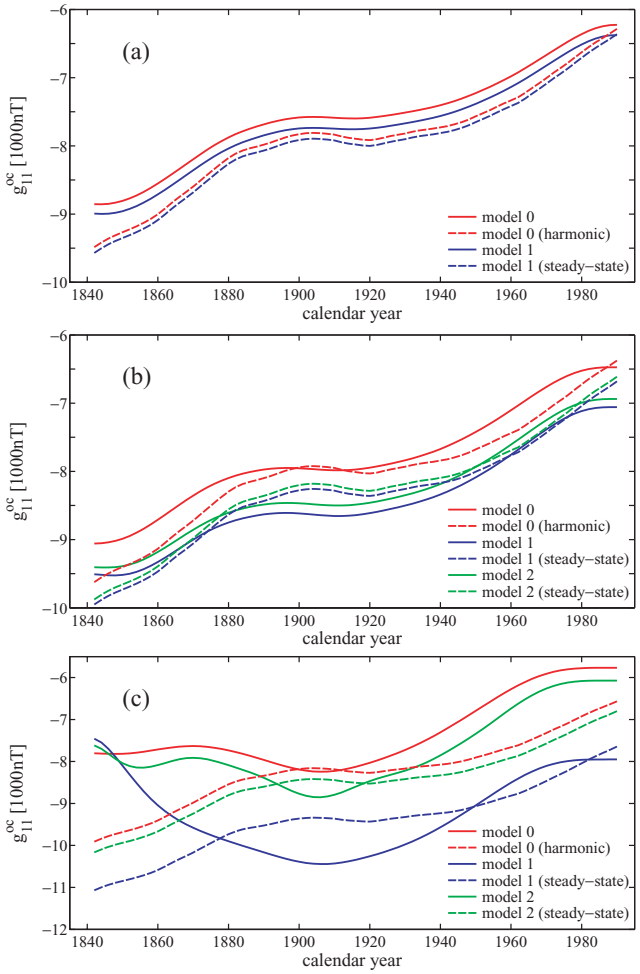

Figure 3. Spherical harmonic coefficient g_{11}^{oc} continued by diffusive, harmonic and steady-state downward continuation to the spheres $r = R_{oc}$ inside the core for the models of the angular velocity, $\omega(r)$, shown in Fig. 2: (a) $R_{oc} = R_c - 25$ km, (b) $R_{oc} = R_c - 50$ km and (c) $R_{oc} = R_c - 100$ km. Model 2 is not shown in (a) since the difference from model 1 is insignificant.

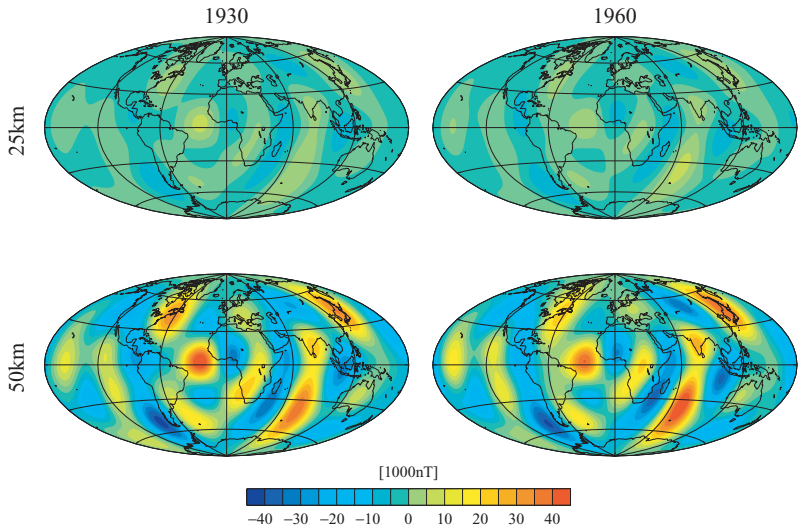

Figure 4. The radial component B_r of the geomagnetic field up to degree and order 8 diffusively continued in the upper core layer. The figure shows the difference between B_r calculated with velocity $\omega(r)$ model 0 and model 1, respectively, for different depths (25 and 50 km) below the CMB at different epochs (1930 and 1960).

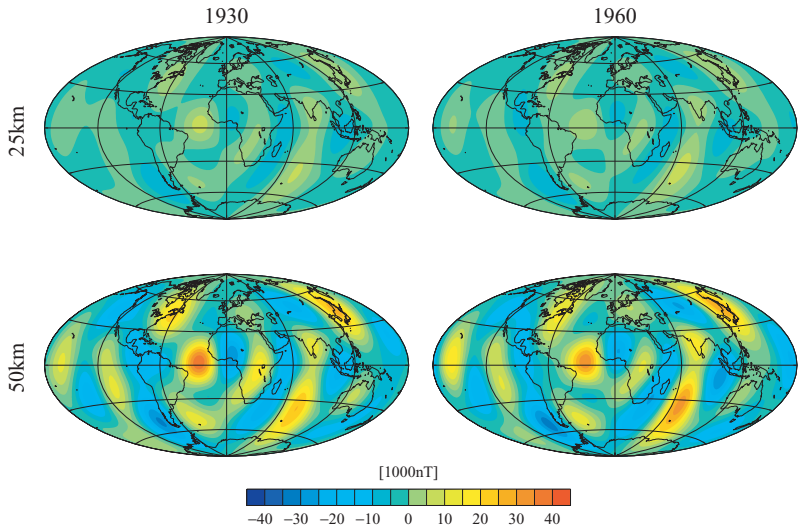

Figure 5. The radial component B_r of the geomagnetic field up to degree and order 8 diffusively continued in the upper core layer. The figure shows the difference between B_r calculated with velocity $\omega(r)$ model 0 and model 2, respectively, for different depths (25 and 50 km) below the CMB at different epochs (1930 and 1960).

differences between the diffusive eqs (27), (25) and the steady-state downward continuations eqs (26), (24) in the core and the influence of the relative rotation on the field variations. The influence of model assumptions about the conductivity has been discussed in a previous paper by Ballani *et al.* (2002) for the mantle and a non-rotating core, i.e. a passive upper core layer (here model 0).

For determining the B_r field in Figs 4 and 5 discussed at the end of this section, we have calculated all coefficients up to $n = 8$, $m = 8$. Because they have nearly the same properties of continuation, it is sufficient to show g_{11} as an example which is representative of the behaviour of the harmonic modes in the outer core:

(i) Fig. 3(c) is used to demonstrate the stability problems of the algorithm and to determine the approximate depth to which the continuation of decadal field variations is possible. The first part of the time interval is dominated by the influence of the required initial condition by which a certain arbitrariness is introduced. Therefore, the irregular behaviour in Fig. 3(c) in the first 40 yr is a typical effect of the regularization procedure. The large amplitudes of the variations in the middle of the curves indicate that the solution of the problem becomes nearly unstable. Instability shall mean here that the range of values can exceed those of the 25 km and 50 km solutions by about one order of magnitude, which is not physically reasonable. In addition, any correlative (spectral) relation to the data and the solutions above is lost. It must be mentioned here that the misfit bound for the data at R_σ, $\epsilon = \|(a_{ik})\,(f_k) - (\phi_i)\|_\alpha$ (see the regularization procedure of eq. 46) is chosen as 5 per cent for $r \geq R_c - 50$ km, corresponding to the assumed error level of the data. This r level is then the maximum depth for which no instabilities appear. For $r = R_c - 100$ km, we need a higher ϵ value (10 per cent) to reach a stable solution, otherwise for $\epsilon = 5$ per cent and radii $r = R_c - 100$ km and deeper the solutions becomes unstable, corresponding to

the typical trade-off in the Tikhonov regularization. From a physical point of view, this behaviour may be associated with crossing the skin depth of decadal variations by downward continuation. Because we are not dealing with single frequencies, this skin depth cannot be quantified by only one value of r and is an interval of radii according to the frequency spectrum of the time series used. In general, the determination of an r-dependent misfit bound ϵ necessary to reach stable solutions, i.e. solutions of physical relevance, has to be found for each case separately.

(ii) We use the solutions for the model 0 (eq. 25) and compare them with their steady-state case (eq. 24), the harmonic one, to demonstrate the absolute effect of the high conductivity in the core (model 0 is defined by $\omega = 0$) on the variations of the poloidal modes. For model 0, one result is a significant phase shift between the solutions in the steady state and diffusive case which increase with depth. Apart from this shift, the solutions show an offset and a remaining mean difference of solutions after shift and offset have been applied, which become significant at the two depths of 25 km and 50 km below the CMB, but do not exceed a maximum value of about 500 nT. A comparison with the solutions for $\omega \neq 0$ (models 1 and 2) shows that the rotation produces no visible additional phase shift, meaning that the shift between the solutions in the diffusive and steady-state cases is mainly a consequence of the high conductivity of the core.

(iii) Comparing the results for the different ω models of eqs (25) and (27), we can conclude that the rotation increases the absolute magnitude of the coefficient (compare models 1, 2 with model 0) by a larger amount than discussed in (ii). Moreover, the difference between model 1 and 2 is marginal at 25 km (this cannot be resolved on the scale of Fig. 3a) but becomes significant at greater depths, as expected from the r dependence shown in Fig. 2, where the angular velocities of models 1 and 2 nearly agree for the first 25 km. As already mentioned in (ii), we cannot see a remarkable phase shift between the models in the diffusive case.

To demonstrate the influence of the relative rotation in the outermost core on a physical quantity completely determined by the diffusively continued poloidal part of the field (eqs 25, 27), we have calculated the differences in $B_r(R_{oc}, \vartheta, \varphi, t)$ (eq. 59) between calculations including model 0 and including models 1, 2, respectively, and shown its distribution over the globe in Figs 4, 5.

Comparing the two figures, we conclude that models 1 and 2 cannot be distinguished at a depth of 25 km beneath the CMB but differ significantly from model 0 there as stated for g_{11} in (ii) above, and the models 1 and 2 differ at 50 km (see e.g. anomalies in North America, East Asia and in the south of India) significantly showing a behaviour comparable to that for g_{11} in (iii) above. In accordance with this, model 1 (Fig. 4) shows larger differences from model 0 than model 2 (Fig. 5).

The differences between the two epochs 1930 and 1960 are not very large but suggest that the difference between the solutions for the moving and the non-moving fluid changes slightly with time. This may be a consequence of a variable time structure in the data.

6 CONCLUSIONS

We have shown that the algorithm by which we recently solved the inverse induction problem for the mantle and a non-moving outer core (Ballani *et al.* 2002) can be extended to the relatively rotating outermost core with small modifications if its angular velocity is approximated with a differential rotation. As the method does not represent a kind of disturbance theory but provides the full inversion free from assumptions about the scale of the magnetic field, it is able to account for the high-conducting core material combined with the prescribed motions, at least down to a depth of 50 km at the 5 per cent level of data error. Nevertheless, for a more realistic velocity field the situation will be more complicated, in particular if the toroidal field needs to be considered. Our investigation should therefore only be understood as a preliminary step in the investigation of the inverse induction problem of the core.

As an example calculation we have shown that the effect of the high conductivity dominates the phase shift by diffusion, whereas the relative rotation has no detectable influence on it. In consistency with the particular r dependence in the prescribed model of $\omega(r)$ the influence of the relative rotation on the magnitude of the magnetic field is marginal in the first 25 km of the outer core, but leads to a significant amplification of the field in deeper parts (and a weakening in the forward problem).

The comparison with the downward continuation in the steady-state cases has shown that the diffusive inverse solution is stable in the first 50 km of the upper core if a data error ϵ of 5per cent at $r = R_\sigma$ is allowed; for 100 km depth, this value must be increased to 10 per cent in order to construct a stable solution for the downward continuation at all. Its physical reasonableness is no longer certain.

Apart from possible physical constraints not considered in this paper, this behaviour is probably related to an r-dependent skin effect appearing if the boundary values are given by a discrete finite time-series with a certain spectral band instead of a single harmonic signal.

The method used can be applied to calculations of geomagnetic variations in the outer core necessary for investigations of the velocity field by frozen-flux theory, calculations of EM torques and estimates of the strength of the magnetic-flux in parts of the outer core. The pure induction effects (e.g. in a passive layer) are known; a further physical interpretation of these problems compared with conventional approximate solutions should be explored in the near future.

ACKNOWLEDGMENTS

We thank our colleagues Jun-Yi Guo (Wuhan University, China), for continuously stimulating discussions, and Monika Korte (GFZ), who suggested some valuable improvements. The detailed reviews of two unknown reviewers are gratefully acknowledged. Their comments and questions helped us to improve the paper distinctly in style and basic details. We are grateful to our colleagues Veronika Söllner and Hans Kühn for their technical support.

REFERENCES

Arfken, G., 1966. *Mathematical Methods for Physicists,* Academic Press, New York.

Backus, G.E., 1983. Application of mantle filter theory to the magnetic jerk of 1969, *Geophys. J. R. astr. Soc.,* **74,** 713–746.

Ballani, L., Greiner-Mai, H. & Stromeyer, D., 1995. Über ein nichtcharakteristisches Cauchy-Problem bei der geomagnetischen Kern-Mantel-Kopplung., *Z. Angew. Math. Mech.,* **75,** 613–614.

Ballani, L., Greiner-Mai, H. & Stromeyer, D., 2002. Determining the magnetic field in the core–mantle-boundary zone by non-harmonic downward continuation, *Geophys. J. Int.,* **149,** 374–389.

Ballani, L., Wardinski, I., Stromeyer, D. & Greiner-Mai, H., 2004. Time structure of the 1991 magnetic jerk in the core–mantle-boundary zone by inverting global magnetic data supported by satellite measurements, in *CHAMP Mission Results from Gravity and Magnetic Field Mapping, and GPS Atmosphere Sounding,* pp. 311–316, eds Reigber, C., Luehr, H., Schwintzer, P. & Wickert, J., Springer-Verlag, Berlin.

Bellanger, E., Le Mouël, J.-L., Mandea, M. & Labrosse, S., 2001. Chandler wobble and geomagnetic jerks, *Phys. Earth Planet. Inter.,* **124,** 95–103.

Benton, E.R. & Whaler, K.A., 1983. Rapid diffusion of the poloidal geomagnetic field through a weakly conducting mantle: a perturbation solution, *Geophys. J. R. astr. Soc.,* **75,** 77–100.

Bloxham, J. & Jackson, A., 1992. Time-dependent mapping of the magnetic field at the core–mantle boundary, *J. geophys. Res.,* **97,** 19 537–19 563.

Braginsky, S.I., 1993. MAC oscillations of the hidden ocean of the core, *J. Geomag. Geoelectr.,* **45,** 1517–1538.

Buffett, B.A., 1992. Constraints on magnetic energy and mantle conductivity from the forced nutations of the Earth, *J. geophys. Res.,* **97,** 19 581–19 597.

Buffett, B.A., Jeanloz, R. & Garnero, E., 2000. Sediments at the top of Earth's core, *Science,* **290,** 5495–5497.

Buffett, B.A., Mathews, P.M., & Herring, T.A., 2002. Modeling of nutation and precession: effects of electromagnetic coupling, *J. geophys. Res.,* **107,** doi:10.1029/2000JB000056.

Dinh Nho Hào & Gorenflo, R., 1991. A noncharacteristic Cauchy problem for the heat equation, *Acta Appl. Math.,* **24,** 1–27.

Dubrovinsky, L. et al 2003. Iron–silica interaction at extreme conditions and the electrically conducting layer at the base of Earth's mantle, *Nature,* **422,** 58–61.

Eldén, L., 1995. Numerical solution of the sideways heat equation, in *Inverse Problems in Diffusion Processes,* pp. 130–150, eds Engl, H. & Rundell, W., Philadelphia, SIAM.

Greiner-Mai, H., 1986. Westward drift of the Earth's core and the Earth's rotation, *Gerlands Beitr. Geophys.,* **95,** 341–354.

Greiner-Mai, H., 1995. About possible geophysical causes of the decade fluctuations in the length of day, *Astron. Nachr.,* **316,** 311–318.

Gubbins, D., 1996. A formalism for the inversion of geomagnetic data for core motions with diffusion, *Phys. Earth planet. Inter.,* **98,** 193–206.

Hansen, P.C., 1994. *Regularization Tools. A Matlab Package for Analysis and Solution of Discrete Ill-Posed Problems,* Numerical Algorithms, 6, 1–35.

Holme, R., 1998. Electromagnetic core-mantle coupling—II. Probing deep mantle conductance, in *The Core–Mantle Boundary Region*. pp. 139–151, eds Gurnis, M., Wysession, M.E., Knittle, E. & Buffett, B.A., American Geophysical Union, Washington, DC.

Krause, F. & Rädler, K.H., 1980. *Mean Field Magnetohydrodynamics and Dynamo Theory,* Akademie Verlag, Berlin.

Lay, T., Williams, Q. & Garnero, E.J., 1998. The core–mantle boundary layer and deep Earth dynamics, *Nature,* **392,** 461–468.

Reinhardt, H.-J. & Seiffarth, F., 1993. On the approximate solution of illposed Cauchy problems for parabolic differential equations, in *Inverse Problems: Principles an Applications in Geophysics, Technology, and Medicine,* pp. 284–298, eds Anger, G., Gorenflo, R., Jochmann, H., Moritz, H. & Webers, W., Akademie Verlag, Berlin.

Shankland, T.J., Peyronneau, J. & Poirier, J.-P., 1993. Electrical conductivity of the Earth's lower mantle, *Nature,* **366,** 453–455.

Stefani, F. & Gerbeth, G., 2000a. Can we look inside a dynamo?, *Astron. Nachr.,* **321,** 235–247.

Stefani, F. & Gerbeth, G., 2000b. On the uniqueness of velocity reconstruction in conducting fluids from measurements of induced electromagnetic fields, *Inverse Problems,* **16,** 1–9.

Stromeyer, D., 1983. Methodische Untersuchungen zur Inversion geothermischer Daten, *PhD thesis,* Forschungsbereich Geo- und Kosmoswissenschaften, Potsdam.

Stromeyer, D., 1984. Downward continuation of heat flow data by means of the least squares method, *Tectonophysics,* **103,** 55–66.

Tanaka, S. & Hamaguchi, H., 1993. Velocities and Chemical Stratification in the Outermost Core, *J. Geomag. Geoelectr.,* **45,** 1287–1301.